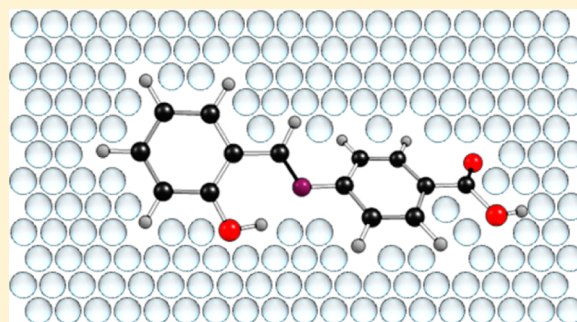


Structure and Photochemistry of *N*-Salicylidene-*p*-carboxyaniline Isolated in Solid Argon

Mihaela Avadanei,[†] Nihal Kuş,^{‡,§} Vasile Cozan,[†] and Rui Fausto^{*,‡}[†]“P. Poni” Institute of Macromolecular Chemistry, 700487 Iasi, Romania[‡]Department of Chemistry, University of Coimbra, 3004-535 Coimbra, Portugal[§]Department of Physics, Anadolu University, 26470 Eskişehir, Turkey

S Supporting Information

ABSTRACT: Infrared matrix isolation spectroscopy and DFT/B3LYP/6-311++G(d,p) calculations have been used to characterize the conformational space of the enol-imine and keto-amine tautomers of *N*-salicylidene-*p*-carboxyaniline (SCA) in both their *E* and *Z* isomeric forms. Monomers of SCA were isolated in an argon matrix (15 K), which was shown to contain only the most stable conformer of the *E*-enol isomer of the compound. The matrix-isolated *E*-enol was then subjected to *in situ* UV irradiation ($\lambda = 335$; 345 nm, provided by a laser/MOPO system, or $\lambda > 235$ nm, provided by a Hg(Xe) broad-band source), and the photoinduced processes probed by infrared spectroscopy. Two photoreaction channels were observed, with a branching ratio of $\sim 1:1$, corresponding to *E*-enol \rightarrow *Z*-enol isomerization and *E*-enol \rightarrow *E*-keto tautomerization. Both processes were found to be rather effective, with practically complete consumption of the reactant after broad-band irradiation by 1 min only. Identification among the photoproducted species of the *Z*-enol conformer that differs from the reactant only by *E*-to-*Z* isomerization suggests the initial photoproduction of this conformer, which subsequently decays into the lowest energy *Z*-enol conformer (also identified experimentally). The *E*-enol \rightarrow *E*-keto tautomerization requires an excited state intramolecular proton transfer and twisting about the exocyclic CC bond of the molecule. These processes most probably take place sequentially. However, in the present study the *Z*-keto isomer, which should act as intermediate in this sequence of processes, could not be detected, most probably due to its short lifetime under the used experimental conditions. On the contrary, the detailed structural and vibrational characterization of the photoproducted *E*-keto form was successfully achieved.



1. INTRODUCTION

The *N*-salicylidene anilines (SA; Scheme 1) belong to the *o*-hydroxyaryl Schiff bases family and constitute a special class of organic materials showing switchable properties triggered by light, such as photochromism and photoluminescence, which can be efficiently exploited in practical applications like fast molecular photoswitches, optical storages, and molecular machines.^{1–3} These molecules have an internal hydrogen bond involving the phenolic and the azomethine groups that facilitates intramolecular proton transfer, thus allowing the existence of two tautomeric forms: enol-imine and keto-amine. In turn, each of these tautomers has two geometrical isomers (*E* and *Z* forms), defined around the exocyclic C=N (enol-imine tautomer) or C=C bond (keto-amine tautomer), which may possess several conformational isomers.

For most of *N*-salicylidene anilines, the ground state is populated by the *E*-enol form, which is stabilized by an O—H \cdots N intramolecular hydrogen bond that also locks the salicylidene unit in a nearly planar conformation. The rich photochemistry, in particular the photochromism exhibited by these compounds, relies on a complicated succession of events,

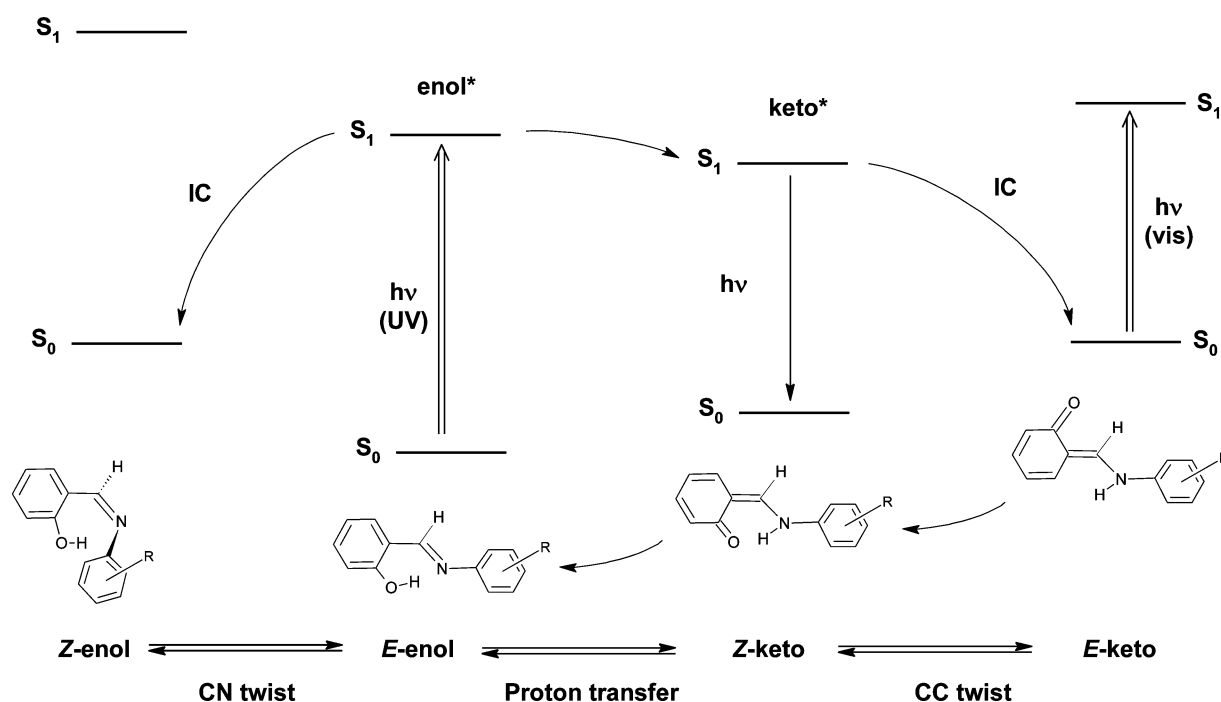
following the electronic excitation of the *E*-enol form with UV light (Scheme 1).

Salicylidene aniline derivatives change from yellow to red upon irradiation with UV light and back to the original yellow upon exposure to heat (thermal fading) or visible light. The photochromic cycle can be described by the succession: light absorption to the first excited (S_1 , π , π^*) state of the *E*-enol \rightarrow excited state proton transfer (ESIPT),^{4–7} leading to the *Z*-keto form \rightarrow isomerization to the chromophoric *E*-keto form/emission \rightarrow thermal isomerization and back proton transfer in the ground state, with recovery of the proton by the phenolic group and restoring of the initial enolic form.^{8–13} The proton transfer process triggers a suite of geometrical changes, starting with the loss of aromaticity in the phenolic moiety through tautomerization, and ending with the isomerization into the final chromophoric *E*-keto structure.

The phototautomerization can be accompanied by an *E* \rightarrow *Z* isomerization around the azomethine C=N bond, which

Received: July 7, 2015

Revised: August 4, 2015

Scheme 1. General Scheme of the Photochemistry of *N*-Salicylidene Anilines

brings a twisted conformation of the enol form. Predicted theoretically for the salicylidene aniline parent compound,^{6,11} the *Z*-enol isomer has been connected with a remnant negative band observed in the transient absorption spectra, on the UV wing, for *N,N'*-bis(salicylidene)-*p*-phenylenediamine,¹⁴ bis((phenylimino)methyl)hydroquinone, and 4-methoxy-2,5-bis((phenylimino)methyl)phenol.¹⁵ An infrared spectroscopic proof of the twisted geometry has been recently reported for 2-(1-(methylimino)methyl)phenol isolated in an argon matrix.¹⁶

The chemical structure of the colored photoproduct, although widely recognized as the *E*-ketonic species, is still a matter of some debate. It has been considered that the neutral quinoid form can coexist with a zwitterionic form,¹⁷ and that the dominance and lifetime of one particular structure depend on the molecular surroundings.

The characteristic photodynamics of *N*-salicylidene anilines can become more complex due to the existence of further isomers and conformers of both the starting compound and the transient species, and also due to competing radiative and nonradiative channels. Thus, creation of the *Z*-enol and the chromophoric *E*-keto photoproducts takes place through two S_1/S_0 conical intersections (CI), reached in a barrierless mode by rotation around the exocyclic C=N and C=C bonds, respectively (Scheme 1). Deactivation of the $S_1(\pi,\pi^*)$ state of the *Z*-keto form through fluorescence is concurrent with the internal conversion through the S_1/S_0 CI, and the preferred de-excitation pathway is determined by details of the chemical structures and medium factors.

Because of the multiple events at the excited state level, the photochromic cycle of SA derivatives has been mainly studied by electronic absorption and fluorescence spectroscopy, using steady state or time-resolved techniques. Conventional^{18,19} and time-resolved infrared spectroscopy^{20,21} were used to identify the photoproducts of irradiated salicylidene aniline in solution, polycrystalline film and engaged in zeolites.

One of the most important features of the photochromic compounds is the fact that their photodynamics and photo-reactivity can be controlled by molecular environment and chemical substitution. From this perspective, minimizing the intermolecular interactions and inhibiting molecular diffusion is desirable to investigate the photophysical events without external influences. These conditions are readily available by isolating the molecules of the target compounds in low temperature cryogenic noble gas matrixes. However, studies on matrix isolated Schiff bases are scarce and have been essentially centered on the analysis of conformational characteristics of the molecules and hydrogen bonding aspects.^{22–24} To the best of our knowledge, only a few studies have been concerned with the photochemical transformations of these molecules.^{16,25}

The present investigation focused on the photoinduced structural changes of *N*-salicylidene-*p*-carboxyaniline (abbreviated, SCA) isolated in a solid argon matrix. Although the photochromic behavior of SCA in the crystalline state is known, and shown to be governed by the packing arrangement,²⁶ the unimolecular photochemistry of SCA had never been addressed hitherto.

The well-known photochromism exhibited by the parent compound, salicylidene aniline, in the solid phase,²⁷ is considered to be related with the large deviation (36°) of the two aromatic rings from planarity, which “prepares” the molecule for the *E*–*Z* isomerization. On the contrary, due to the terminal –COOH group, SCA has the ability to self-associate in the solid state as dimers.²⁶ The presence of the neutral *E*-enol form in the ground state was confirmed by X-ray diffraction and infrared spectroscopy data.²⁶ In the crystalline state, the SCA molecules adopt an almost flat geometry, the dihedral angle between the two aromatic rings being only $7.8(3)^\circ$. The claim resulting from former studies that SCA did not exhibit photochromism in solid state^{27–29} was then attributed to the almost planar conformation and crowded packing in the crystal. However, in contrast to those studies, our recent study has revealed that the compound is effectively

photochromic in the solid state.²⁶ The relative good quantum yield of fluorescence in the crystalline state (0.115),²⁶ combined with the photochromic behavior, seems to indicate a quite unusual behavior under light excitation that is worth investigating.

In the present study, SCA was isolated in an argon matrix, at 15 K, and irradiated with laser light ($\lambda = 335, 345$ nm) or with the full wavelength range of a high-pressure Hg(Xe) lamp. Establishing the structure of SCA species present in the cryogenic matrix and the photoproducts identification were assisted by quantum chemical calculations carried out at the DFT/B3LYP/6-311++G(d,p) level of approximation. Besides the detailed structural analysis of the potential energy surface of the compound and of the vibrational spectra of its possible isomeric forms, this study provides relevant details on the photochemical transformations of the isolated molecule of SCA, thus also contributing to further our understanding of the general photochemistry of *N*-salicylidene anilines.

2. EXPERIMENTAL AND COMPUTATIONAL METHODS

2.1. Synthesis. The synthesis of SCA has been described in a previous publication.²⁶ Briefly, stoichiometric amounts of salicylaldehyde and carboxybenzaldehyde were allowed to react in ethanol, at room temperature, for 5 h. The solvent was removed, and the remained solid product was washed with ethanol three times, affording a pure and yellow crystalline powder. Ethanol (Chimopar SA) and the starting materials (Sigma-Aldrich) were used as received.

2.2. Matrix-Isolation FTIR Spectroscopy. SCA was deposited by sublimation from a specially designed Knudsen cell together with a large excess of the matrix gas (Ar, N60 purity, from Air Liquide) onto a CsI window, cooled at 15 K. An APD Cryogenics closed-cycle helium refrigeration system with a DE-202A expander was used. The temperature of the CsI window was measured directly at the sample holder by a silicon diode sensor, connected to a digital temperature controller (Scientific Instruments, model 9650-1), which provides an accuracy of 0.1 deg.

The infrared spectra were recorded, in the 4000–500 cm^{-1} range, using a Nicolet 6700 FTIR spectrometer, equipped with a Ge/KBr beam splitter and a deuterated triglycine sulfate (DTGS) detector. The spectral resolution used was 0.5 cm^{-1} .

2.3. Laser and Broad-Band UV Irradiation Experiments. In a first experiment, the matrix was irradiated using narrow-band tunable light (0.2 cm^{-1} spectral width; repetition rate = 10 Hz; pulse energy 1–2 mJ) provided by the frequency-doubled signal-beam of a Quanta-Ray MOPO-SL optical parametric oscillator, pumped with a pulsed (10 ns) Nd:YAG laser. In a second experiment, the irradiation has been performed through the outer KBr window of the cryostat ($\lambda > 235$ nm) with the broad-band wavelength profile of a 150 W high-pressure Hg(Xe) lamp (Osram XBO 150 W/CR OFR).

2.4. Theoretical Calculations. All molecular geometries were optimized at the DFT level using the B3LYP functional, which includes the Becke's gradient exchange–correction³⁰ and the Lee, Yang, and Parr correlation functionals,³¹ and the 6-311++G(d,p) basis set.³² Vibrational spectra were calculated at the same level of theory. The theoretical frequencies were scaled down by a factor of 0.978 in the fingerprint region, and by 0.945 in the high frequency range. All the calculations were performed with the Gaussian 09 suite of programs.³³

3. RESULTS AND DISCUSSION

3.1. Geometrical Features and Energies of SCA Tautomeric Forms. The enol form of SCA has six internal axes of rotation that may give rise to different isomers. Three of these axes are defined within the salicylidene–azomethine fragment $[(\text{C}_6\text{H}_4\text{OH})\text{CH}=\text{N}]$, corresponding to internal rotations around the C–O phenolic and C=N azomethinic bonds, as well as around the C–C bond connecting the azomethine moiety to the phenolic ring. In the *p*-carboxyphenyl fragment $[(\text{C}_6\text{H}_4)\text{COOH}]$, two internal rotations shall be considered, the first being defined around the C–C bond connecting the carboxylic substituent to the ring, and the second corresponding to the rotation around the carboxylic C–O bond. The sixth internal rotation axis corresponds to the N–C bond connecting the salicylidene–azomethine and *p*-carboxyphenyl fragments. Though *a priori* the molecule appears to be rather complicated in terms of possible geometry arrangements, the situation is in fact relatively simple: (i) The internal rotation about the carboxylic C–O bond leads only to two minimum energy conformations, where the O=C–O–H dihedral takes the values of 0° (*cis*) or 180° (*trans*), the latter corresponding to a high-energy configuration with a relative energy above the most stable geometry that exceeds 40 kJ mol^{-1} and, thus, being of no practical relevance.^{34–36} (ii) The internal rotation about the C–C bond connecting the carboxylic substituent to the ring, for a *cis* arrangement of the O=C–O–H fragment, gives rise to only two minima, where the carboxylic substituent is in the same plane of the aromatic ring.³⁷ The two minima can be expected to have close energies and they must be both considered in the structural analysis of the molecule. (iii) Both the orientation of the phenolic OH group and the preferred geometry around the C–C bond connecting the azomethine and phenolic moieties are essentially determined by the possibility of establishment of the O–H...N intramolecular hydrogen bond, so that the most favorable arrangements of this fragment of the molecule can be easily predicted, corresponding to a nearly planar geometry where the intramolecular hydrogen bond participates in a pseudoaromatic six-membered ring. (iv) Finally, considering the internal planarity of both the salicylidene–azomethine and *p*-carboxyphenyl fragments, the rotation about the N–C bond connecting these two moieties can be easily perceived to lead to the same minimum energy structures as the internal rotation about the C–C bond connecting the carboxylic substituent to the ring. The preferred geometry about the N–C bond can be expected to have the salicylidene–azomethine and *p*-carboxyphenyl fragments in different planes, taking as reference what has been found for other molecules bearing similar structural elements.^{28,29} Considering points (i)–(iv) above, it can be concluded that the number of relevant structures for each enol isomer (*E* and *Z* forms, which are defined by the orientation of the groups around the C=N bond) is in fact rather small.

The situation is even simpler for the keto tautomers of SCA, because the internal rotation associated with the phenolic OH group is lost in this case. The analysis made above in relation to the internal rotations related with the carboxylic substituent applies also to the keto tautomer, as well as that concerning the rotation around the N–C bond. Because the geometry about the exocyclic C=C bond of the keto tautomer defines the nature of each keto isomer (*E* and *Z*), only the rotation around the central C–N bond is distinctive in the keto forms

(compared to the enol forms) and, thus, must be investigated with more detail.

The DFT(B3LYP)/6-311++G(d,p) calculated relative energies of the relevant structures of SCA, for both enol and keto forms, are given in Table 1. Graphical representations of the optimized minimum energy structures are shown in Figure 1A–C.

Table 1. Calculated Relative Energies (ΔE), Zero-Point-Corrected Energies [$\Delta E(0)$], and Gibbs Energies at 298.15 K (ΔG°) for the Different Forms of SCA Enol and Keto Tautomers^a

structure	ΔE	$\Delta E(0)$	ΔG°	ΔE	$\Delta E(0)$	ΔG°
<i>E</i> -enol						
I	0.00	0.00	0.00			
II	0.31	0.25	0.16			
III	51.99	49.21	46.52			
IV	52.06	49.16	46.54			
V	44.51	41.91	39.46			
VI	44.30	41.74	39.30			
VII	36.02	33.35	30.72			
VIII	35.86	33.19	30.48			
<i>Z</i> -enol						
I	63.49	61.68	60.52	2.63	2.35	3.85
II	63.60	61.85	60.75	2.73	2.52	4.07
III	68.65	66.46	65.25	7.79	7.14	8.57
IV	68.67	66.61	65.39	7.80	7.28	8.72
V	66.91	65.00	62.54	6.04	5.68	5.87
VI	66.92	65.02	62.47	6.05	5.69	5.80
VII	60.86	59.33	56.67	0.00	0.00	0.00
VIII	60.91	59.36	56.75	0.04	0.03	0.08
<i>E</i> -keto						
I	62.48	61.32	57.86	0.51	0.48	0.27
II	61.96	60.85	57.59	0.00	0.00	0.00
III	87.48	87.56	85.49	25.51	26.72	27.90
IV	87.21	87.29	85.16	25.25	26.44	27.57
<i>Z</i> -keto						
I	19.70	18.39	16.57	0.00	0.00	0.00
II	20.23	19.09	17.18	0.53	0.70	0.61
III	94.61	94.47	94.20	74.91	76.07	77.63
IV	94.18	94.05	93.83	74.48	75.66	77.26

^aAll energies in kJ mol^{-1} . For structures of the different forms, see Figure 1A–C. The first set of energy values are relative to the most stable form (*E*-enol conformer I); the second set are relative to the most stable conformer of the specific isomer.

As shown in Table 1, and in consonance with the expectations, the calculations predict the most stable conformer of the *E*-enol form as the lowest energy species among all possible structures. In this conformer, the phenolic group is hydrogen bonded to the azomethine nitrogen atom, forming a nearly planar pseudoaromatic six-membered ring ($\text{OH}\cdots\text{N}$ distance: 1.755 Å), and the *p*-carboxyphenyl moiety is also nearly planar, with the carboxylic group assuming the *cis* configuration. The planes of the salicylidene–azomethine and *p*-carboxyphenyl fragments are twisted by $\sim 39^\circ$, with the carbonyl bond of the *p*-carboxyphenyl group pointing to the same side of the $\text{C}=\text{N}$ bond (Figure 1A). As anticipated, the *E*-enol form differing from the lowest energy structure only in the orientation of the carboxylic substituent is almost isoenergetic to this latter ($\Delta E = 0.31 \text{ kJ mol}^{-1}$). All other conformers of the *E*-enol tautomer of SCA (forms III to VIII in

Figure 1A) are comparatively much higher in energy (by over 35 kJ mol^{-1} ; Table 1), mostly due to the breaking of the intramolecular $\text{O}=\text{H}\cdots\text{N}$ bond in the salicylidene–azomethine fragment. The slightly lower relative energies of forms VII and VIII, compared to the energies of forms III–VI, result from the presence in forms VII and VIII of the energetically more favorable $\text{CH}\cdots\text{N}$ and $\text{CH}\cdots\text{OH}$ interactions within the salicylidene–azomethine fragment, as compared to the $\text{CH}\cdots\text{N}$ and $\text{CH}\cdots\text{H}(\text{O})$ interactions existing in forms V and VI, or $\text{CH}\cdots\text{HC}$ and $\text{N}\cdots\text{OH}$ contacts shown by forms III and IV.

The *Z*-enol isomer has also eight conformers, which correlate directly with the eight conformers of the *E*-enol isomer above-discussed. As for this latter isomer, the *Z*-enol conformers can be grouped in pairs showing identical structures except in the orientation of the carboxylic group. The members of each group are also practically isoenergetic (Table 1). Compared to the most stable *E*-enol form, all *Z*-enol conformers have energies above 60 kJ mol^{-1} . The *Z*-enol conformer differing from the most stable *E*-enol conformer essentially by isomerization about the $\text{C}=\text{N}$ bond (*Z*-enol I) is the third more stable *Z*-enol form and bears a weak $\text{O}=\text{H}\cdots\pi$ intramolecular hydrogen bond, established between the phenolic OH group and the *p*-carboxyphenyl aromatic ring. This conformer is 2.6 kJ mol^{-1} higher in energy than the lowest energy *Z*-enol conformer (*Z*-enol VII), which differs from *Z*-enol I in the orientation of the OH phenolic group and by rotation about the $\text{C}-\text{C}$ bond connecting the phenol moiety to the azomethine group (Figure 1B). This arrangement grants a more opened structure that is also stabilized by a $\text{C}-\text{H}\cdots\text{O}(\text{H})$ contact. The pairs of *Z*-enol conformers III/IV and V/VI have higher energies (over 6 kJ mol^{-1} above the most stable *Z*-enol conformer) because they bear less favorable $\text{HO}\cdots\pi$ and $\text{OH}\cdots\text{H}$ contacts, respectively. All *Z*-enol conformers are strongly nonplanar, with the planes between the azomethine and *p*-carboxyphenyl fragments and between the azomethine and phenol fragments twisted by $56\text{--}68^\circ$ and $23\text{--}43^\circ$, respectively. The geometry around the $\text{C}=\text{N}$ double bond is also slightly deviated from planarity in all forms ($6\text{--}8^\circ$), as suggested before for similar compounds.^{6,11,14–16} On the contrary, the phenolic OH group is deviated significantly from the plane of the aromatic ring only in conformers I/II ($\sim 19^\circ$) and V/VI ($\sim 8^\circ$), where it is pointing inside the molecule, whereas in the *Z*-enol conformers III/IV and VII/VIII, where it points outside the molecule, it is deviated from the ring plane by less than 3° .

In the case of the keto tautomer of SCA, the calculations indicate that the *Z* isomer is considerably lower in energy than the *E* form (by over 40 kJ mol^{-1}), as it could be anticipated by taking into account that the stabilizing intramolecular hydrogen bond ($\text{N}=\text{H}\cdots\text{O}=\text{O}$) present in the *Z*-keto form is not present in the *E*-keto isomer (Figure 1C). As for the enol isomers, for both *E*- and *Z*-keto isomers the conformers differing only in the orientation of the carboxylic group are almost isoenergetic (Table 1). The most stable pair of conformers of the two keto isomers possesses a planar geometry (C_s symmetry point group), with the two substituted rings placed in the opposite sides of the central $\text{C}-\text{N}$ bond. The higher energy forms are nonplanar and have much higher energies compared with the most stable pairs of conformers (by ca. 25 and 75 kJ mol^{-1} , for *E*- and *Z*-keto isomers, respectively; Table 1). These high energies result from the significantly unfavorable interactions between the cyclohexadienone and *p*-carboxyphenyl fragments,

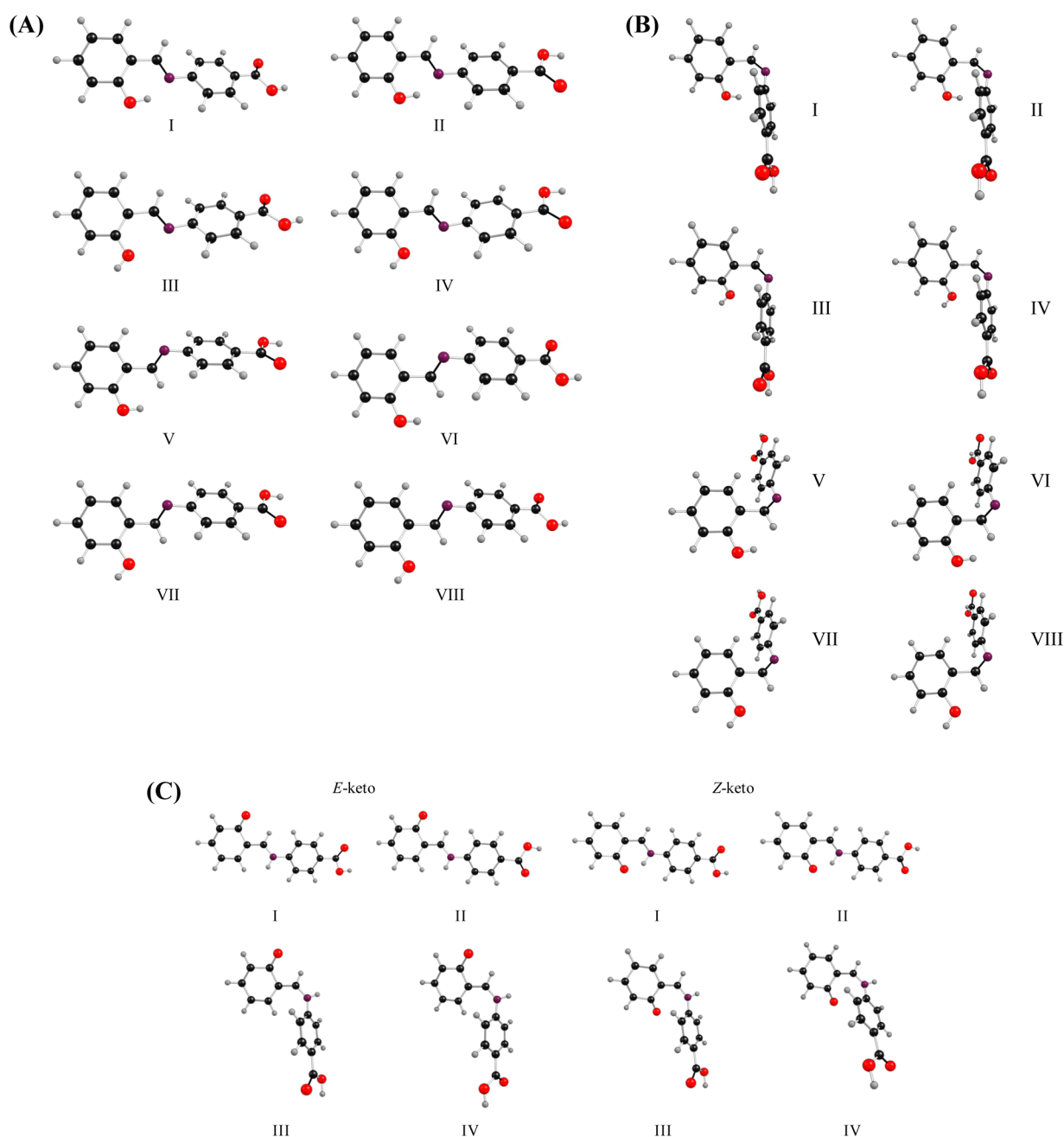


Figure 1. Conformers of (A) the SCA *E*-enol isomer, (B) the SCA *Z*-enol isomer, and (C) the SCA *E*-keto and *Z*-keto isomers. B3LYP/6-311+G(d,p) calculated geometries are provided in the [Supporting Information](#).

which are particularly relevant in the high-energy *Z*-keto isomers, where the oxygen atom of the first fragment is directed toward the aromatic ring of the second.

By comparison of the corresponding most stable conformers, the calculated energy order of the four isomeric forms of SCA is *E*-enol > *Z*-keto ($\sim 20 \text{ kJ mol}^{-1}$) \gg *E*-keto and *Z*-enol ($\sim 60\text{--}62 \text{ kJ mol}^{-1}$). The optimized geometries of all the investigated SCA forms are provided as [Supporting Information](#) (Tables S1 and S2).

3.2. Infrared Spectrum of SCA in an Argon Matrix. The X-ray diffraction data obtained for the SCA starting material²⁶ indicated that, in the crystalline phase, molecules exist in the most stable *E*-enol conformer (I). Because conformer II is almost isoenergetic to conformer I, and all the other conformers of the *E*-enol have energies much higher than

these two forms ($>30 \text{ kJ mol}^{-1}$, if Gibbs energies are considered), it can be expected that, upon sublimation, conformers I and II coexist in the gas phase equilibrium. At room temperature, the expected populations of these two conformers, based on their calculated Gibbs energies (0.16 kJ mol^{-1} ; [Table 1](#)) are I = 52% vs II = 48%.

As a general rule, in a matrix isolation experiment the gas phase conformational equilibrium existing in the gaseous beam used to prepare the matrix can be frozen in the cryogenic media. The populations of the different conformers in the matrix would then be equal to those of the gas phase prior to deposition. However, if two conformers of different energies are separated by low energy barriers (of a few kJ mol^{-1}), conformational cooling usually takes place and the less stable conformer converts into the most stable form during

deposition.^{38,39} This phenomenon makes the information on the energy barriers of great relevance for interpretation of the spectra of matrix isolated species in terms of their conformational composition.

In the case of SCA, the two *E*-enol conformers populated in the gas phase equilibrium at room temperature, forms I and II, can be interconverted by two ways: (i) by rotation around the C–C bond connecting the carboxylic substituent to the ring; (ii) by the rotation about the N–C bond connecting the salicylidene–azomethine and *p*-carboxyphenyl fragments. The potential energy profiles for these two different interconversion pathways are given in Figure 2. As can be seen in this figure, the

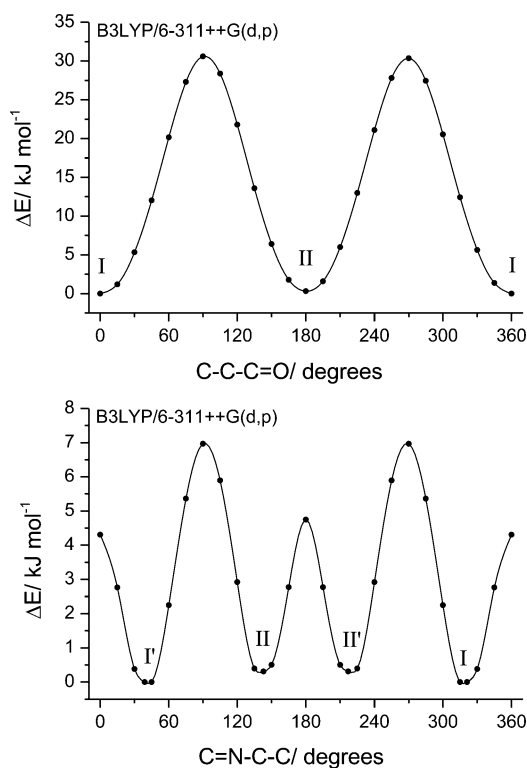


Figure 2. Potential energy profiles for interconversion between the two most stable conformers of the *E*-enol isomer. Top: by internal rotation about the C–C bond connecting the carboxylic substituent to the ring; Bottom: by internal rotation about the N–C bond connecting the salicylidene–azomethine and *p*-carboxyphenyl fragments. (I/I' and II/II' represent pairs of symmetry equivalent conformers.)

barrier associated with the rotation around the C–C bond connecting the carboxylic substituent to the ring is of ca. 30 kJ mol⁻¹; i.e., it is large enough to allow both conformers I and II to be trapped in the matrix. The energy profile for rotation around the N–C bond is more complex, because it shows three different transition states: the two planar transition states (Figure 2) are associated with the conversion between the two pairs of equivalent-by-symmetry forms (I,I' and II,II') and correspond to energy barriers of ca. 4.5–5.0 kJ mol⁻¹; in turn, the transition states where the salicylidene–azomethine and *p*-carboxyphenyl fragments are nearly perpendicular to each other interconvert conformer I into II (or I' into II') and stays ca. 7 kJ mol⁻¹ above the minima. These energy barriers might be low enough to allow for conformational cooling to take place upon deposition of the matrix. Thus, the calculations suggest that most likely only the *E*-enol lowest energy

conformer I shall be present in the as-deposited argon matrix of SCA.

The infrared spectrum of the Ar-matrix isolated SCA is presented in Figure 3 (for the high-frequency range, Figure S1

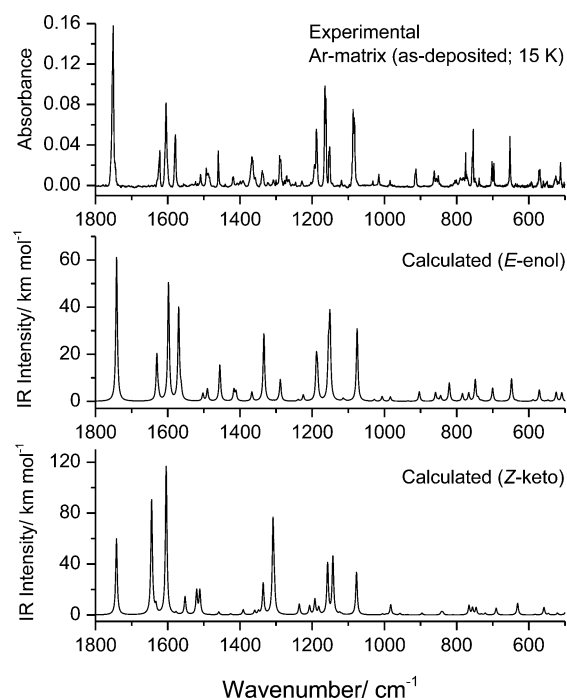


Figure 3. Infrared spectra (in the 1800–500 cm⁻¹ spectral range) of SCA monomers trapped in an argon matrix (15 K; top) and the B3LYP/6-311++G(d,p) calculated spectra of the most stable conformers of the *E*-enol (middle) and *Z*-keto tautomers (bottom). The theoretical wavenumbers were scaled down by a factor of 0.978; bands were simulated by Lorentzian functions centered at the scaled calculated frequency and with full-width-at-half-band of 5 cm⁻¹. Calculated spectra for the most stable conformer of all SCA tautomers are shown in Figure S2 (Supporting Information).

in the Supporting Information). The proposed band assignments are provided in Table 2. As it is shown, the experimental spectrum agrees very well with the theoretical spectrum of the most stable *E*-enol conformer I, doubtlessly confirming the presence of this species in the matrix. The presence of both the *Z*-enol and *E*-keto forms in the spectrum of the as-deposited matrix can be safely excluded, because formation of these species from the *E*-enol can only occur upon photoexcitation. The absence of the *Z*-keto form in the matrix could also be easily confirmed. Indeed, the predicted infrared spectrum of the most stable conformer of the *Z*-keto form of SCA (the one resulting from *E*-enol conformer I by simple proton transfer from the phenol moiety to the nitrogen atom of the azomethine group) has characteristic intense infrared bands at 1644, 1552, 1520, 1511, 1308, and 631 cm⁻¹, which do not have any experimental counterpart (Figure 3). On the contrary, the presence of the *E*-enol conformer II in the matrix cannot be ruled out *a priori*, because the infrared spectra of the *E*-enol conformers I and II are practically coincident (Figure S3). Nevertheless, as discussed above, its absence has been suggested by the theoretical analysis of the potential energy surface of the molecule. To address this question experimentally, the matrix was annealed up to 45 K (in steps of 3 K), to see if any spectral changes were observed that could be

Table 2. Assignment of the Vibrational Spectra of As-Deposited SCA Ar-Matrix and Irradiated Matrix^a

Experimental (Ar matrix)			Calculated			Experimental (irradiated) ^c			Calculated			Calculated		
(as-deposited; 15 K)			E-enol			E-keto			Z-enol VII			Z-enol I		
ν	ν	I^{IR}	Approximate ^b	Description	ν	ν	I^{IR}	Approximate ^b	Description	ν	ν	I^{IR}	Approximate ^b	Description
3577.4/ 3575.1/ 3573.7/ 3572.0/ 3569.4	3565.4	129.1	vOH _c		3632.4					3623.6	93.0	vOH _b		
3225-2625	3072.2	537.9	vOH _b		~3579	3563.9	142.1	vOH		3567.6	113.9	vOH _c	3566.1	114.5
3005.5	3034.6	1.1	vCHCH s r2 (OH)		3540-3490							3542.7	349.0	vOH _b
2999.5	3024.6	1.4	vCHCH s r2 (C=O)			3392.5	20.9	vNH						
2994.5	3022.9	9.5	vCH s r1			3038.5	3.5	v=CH; vCHCH s r2 (OH)		3036.7	2.1	vCH s r1	3033.5	0.8
2984.6	3017.1	12.0	vCH as r1 (m)			3029.5	3.7	v=CH; vCHCH as r2 (OH)		3030.4	1.9	vCHCH s r2 (OH)	3025.0	2.1
2939.8	3012.2	3.6	vCHCH as r2 (OH)			3026.8	0.8	vCHCH as r2 (C=O)		3023.3	2.9	vCHCH s r2 (C=O)	3023.4	8.6
2917.4	3006.2	3.2	vCHCH as r2 (C=O)			3018.4	1.3	v=CH; vCHCH as r2 (OH)		3017.7	8.7	vCH as r1	3016.8	11.2
2899.4	2997.5	7.7	vCH as r1 (p)			3017.4	14.0	vCH s r1		3008.5	2.9	vCHCH as r2 (OH)	3011.1	1.3
2890.0	2986.4	3.3	vCH as r1 (o)			3012.0	14.7	vCH as r1 (m)		3007.8	2.9	vCHCH as r2 (C=O)	3008.3	1.8
2869/ 2862	2872.7	30.8	vCH _{ax}			2986.3	9.0	vCHCH as r2 (C=O)		3003.4	5.1	vCH as r1	3000.3	5.2
1753.5/ 1752.1/ 1751.0	1741.7	482.0	vC=O _c			2984.2	17.0	vCH as r1 (p)		2979.0	14.5	vCH as r1	2987.0	4.6
1621.9	1630.1	154.1	vC=N			2958.8	9.3	vCH as r1 (o)		2949.1	12.0	vCH _{ax}		
1604.7	1625.4	13.4	vCC r1; δ COH _b										2905.9	29.1
1578.9	1597.9	392.6	vCC r1,r2		1747.4	1741.1	504.7	vC=O _c		1736.5	452.3	vC=O _c	1741.9	434.5
	1569.8	310.6	vCC r1; δ COH _b ; vC=N		1668.9					1672.8	260.0	vC=N		
	1563.0	29.1	vCC r2		1661.9	1666.7	483.9	vC=O _c ; vC=C					1664.1	290.7
1509.2	1502.7	25.2	δ CH r2,r1			1618.8	15.1	vCC r1						
1493.2/ 1488.9/ 1485.0	1490.3	40.6	δ CH r1; δ COH _b		1612.2	1611.0	290.1	vCC r2,r1; vC=O _c		1607.6	86.4	vCC r1	1612.5	49.0
1460.4	1455.8	121.0	vCC r1; vCO ₂ δ CH r1		~1605					1599.6	248.5	vCC r2	1600.8	261.5
1419.9/ 1418.2	1416.7	37.6	δ COH _b ; δ CH r1		1593.5	1592.3	198.5	vCC r2,r1 δ NH		1587.9	38.6	vCC r1	1569.7	25.1
1408.0/ 1399.0	1411.1	30.6	vCC r2		1565.0	1559.7	673.7	vC=C; vC=O _c		1554.2	10.3	vCC r2	1554.3	14.4
1358.6	1367.0	30.6	δ CH _{ax}		1530.7	1521.2	426.6	vCC r1						
1366.6/ 1337.8	1333.8	225.7	vC=O _c ; δ COH _b ; vCC(=O)		1515.9	1511.1	350.6	vCC r1,r2		1496.4	8.4	δ CH r1,r2	1493.1	11.7
1322.6	1328.3	0.6	δ CC r1		1477.0					1489.5	23.3	δ CH r1,r2	1478.3	37.4
1308.0	1307.3	0.8	δ CC r2		1463.8	1474.7	52.4	δ NH; vCC r1,r2						
1300.0	1293.9	3.0	δ CH r2		1451.1	1442.5	42.1	vCC r1; δ NH		1455.1	56.4	δ CH r1	1455.4	12.9
1290.3/ 1288.7/ 1287.4	1288.3	71.9	vC=O _b		1414.7	1404.4	11.9	δ CH r2; δ NH		1414.7	46.5	δ CH _{ax}	1409.4	22.0
1246.3	1238.9	4.7	δ CH r1; δ CH _{ax} ; vNC		1414.7	1387.4	0.5	δ CH r1		1411.9	11.2	vCC r2	1404.8	16.6
1228.4	1224.8	20.5	δ CH r1		1362.1	1337.9	100.4	δ COH; vC=O						
1193.4/ 1188.4	1188.5	128.3	δ CH r2; vCC(H)		1327.0	1324.7	224.4	δ CH r1; δ =CH		1332.0	182.9	δ COH _c	1333.4	195.0
1186.6	1185.4	81.1	δ COH _b ; vCC(=O); vC=O _c		1314.2	1317.4	77.6	vCC r2		1327.8	49.0	δ COH _b	1330.0	2.4
1164.6/ 1161.7	1154.9	153.6	δ CH r2; δ COH _c		1302.5	1307.3	91.2	δ CH r2		1304.2	3.9	δ CH r2	1303.8	0.9
1153.4/ 1151.6	1150.9	261.2	δ CH r1; δ COH _c		1298.3					1298.3	67.6	δ CH r1	1301.7	20.8
1119.1	1114.6	7.6	δ CH r1		1293.7	1291.6	711.1	vCN		1289.0	2.8	δ CH r2	1288.1	4.0
1110.3	1109.9	2.4	δ CH r2		1258.0					1243.7	67.3	vC=O _b	1237.9	30.5
1086.8/ 1085.0/ 1083.8/ 1082.6	1075.7	242.6	vC=O _c ; δ CC r1		1242.5	1241.6	18.9	δ =CH					1208.0	30.6
1032.0	1028.0	5.5	vCC r1		1233.2									
1016.7/ 1015.3	1006.5	15.9	δ CC r2		1217.3	1218.1	25.3	vNC		1205.5	8.5	vNC	1194.0	104.9
984.7	983.6	14.6	γ CH _{ax}		1208.0					1187.1	122.3	δ COH _c	1184.2	67.8
979.2	976.0	0.5	γ CH r2		1201.3	1194.6	50.0	δ CH r2; δ COH		1177.8	2.3	δ COH _c ; nCC(HN)		
974.6	968.5	0.3	γ CH r1			1182.1	17.8	δ CH r1						
972.5	966.3	0.2	γ CH r2		1171.3					1168.2	54.6	δ COH _b	1160.8	64.1
937.1	934.7	1.3	γ CH r1		1158.9	1160.1	426.7	δ COH; δ CH r2		1157.9	10.0	δ CH r1		
914.6/ 912.6	903.6	31.9	δ CC r1; δ C(H)NC		1156.2					1148.1	417.3	δ CH r2		
863.9/ 862.0	858.6	28.3	γ CH r2		1146.3	1143.6	110.0	δ CH r1					1153.8	202.1
857.5/ 854.9	852.2	4.4	γ CH r1		1123.7	1119.0	20.9	δ CH r2					1138.8	56.5
851.1	844.5	17.7	vNC _c ; δ CC r2		1093.3	1088.5	16.5	δ CC r1		1108.5	2.5	δ CH r2	1107.1	1.5
816.9/ 814.0	827.7	0.8	γ CH r2		1080.5	1076.1	258.0	vC=O _b ; δ COH		1085.1	36.6	δ CC r1	1099.6	2.6
808.6/ 805.0/ 801.5/ 798.2	820.4	60.8	τ C=O _b		1053.5					1070.1	237.7	vC=O _c	1073.5	221.0
789.9/ 782.2	784.1	25.2	δ CC r1; γ C=O			1003.9	5.0	δ CC r2		1042.8	2.4	vCC r1	1035.4	7.7
775.7/ 771.8	766.7	27.0	γ C=O		1023.2	982.1	0.4	γ CH r1		1005.8	14.6	δ CC r2	1005.7	14.0
757.0/ 754.7	748.6	71.8	γ CH r1		1013.3	982.1	3.1	vCC r1						
749.9/ 748.0	740.1	9.4	vCC(=O); δ COH _c		1008.0	969.9	1.1	γ CH r2		973.7	0.1	γ CH r2	978.5	0.0
738.0	731.0	2.1	τ CC r1		993.3	962.3	1.8	γ CH r2		970.9	1.7	γ CH r2	970.5	0.2
702.3/ 697.5	700.5	44.1	τ CC r2		987.0	954.0	8.4	γ =CH		962.0	1.4	γ CH r2	963.6	0.1
652.7	648.0	75.2	δ OCO		981.7	924.9	0.1	γ CH r1		958.8	6.0	γ CH _{ax}	954.8	4.9
637.5	635.0	1.8	δ CC r2		891.7					933.3	6.4	γ CH r1	934.2	3.0
597.3/ 593.3	588.7	4.7	δ CC r1		873.8	876.7	2.6	δ CC r1		863.0	47.5	τ CC r2	878.9	35.1
572.6/ 570.3	571.2	37.9	τ C=O _c		863.0	857.4	2.0	δ CC r1,r2		841.2	15.7	γ CH r1	856.1	16.6
560.5	553.2	1.1	δ CC r1		843.9	839.0	42.7	γ CH r1,r2		835.5	18.0	τ CC r1	850.2	1.4
550.4	547.1	3.7	τ CC r1			836.5	1.2	γ CH r1,r2		825.6	0.8	γ CH r2	828.6	0.1
525.7	524.5	30.2	δ CN; τ C=O _c			809.6	0.7	γ CH r2		815.9	3.0	δ CC r1,r2	809.3	25.7
512.5	509.0	28.9	τ CC r1,r2		794.1					798.2	5.0	δ CC r2	783.0	33.8
					769.2	778.9	82.9	δ CC r1,r2; δ C=N		772.0	30.8	γ C=O	764.7	4.2
					754.5	763.8	62.3	γ C=O _c		746.5	66.4	γ CH r1	750.3	57.2
						743.5	29.1	τ CC r1						
						730.2	20.5	γ CH r1						
						725.7	6.3	vCC(=O) _c ; δ OCO		725.0	8.6	τ CC r1	720.7	7.7
					711.5					706.5	35.4	τ CC r2	706.8	53.8
					705.9					700.4	30.6	vCC(=O)	698.1	33.0
					693.6	689.5	41.0	τ CC r2						
					670.3					659.1	16.7	δ C=NC	668.9	17.5
						635.8	0.6	δ CC r2		635.1	1.0	δ CC r2	635.2	0.8
					640.6	632.2	52.9	γ NH						
					628.8	623.5	64.9							

ascribed to conversion of conformer II into the most stable form I. According to the Barnes' relationship (which is a well-established empirical correlation relating the size of the energy barrier with the temperature required to start observing a rotamerization process for a matrix isolated molecule),⁴⁰ for a barrier of 7 kJ mol⁻¹ the isomerization should start to be observed at a temperature below 35 K. However, until $T = 39$ K, no relevant spectral changes were observed. Above this temperature evaporation of the argon started to take place (at 45 K, all argon has evaporated), and aggregation of the compound occurred. Formation of molecular associates through the terminal carboxylic group is suggested by the disappearance of the $\nu(\text{C}=\text{O})$ absorption at ca. 1751 cm⁻¹ and its replacement with the broad band at 1699 cm⁻¹. Similarly, the $\nu(\text{OH})$ band at ca. 3574 cm⁻¹ converts into the wider and asymmetric band centered at 3394 cm⁻¹. These changes are accompanied by the transformation of the entire spectrum, with most of the bands observed at 45 K showing a correspondence with those observed in the room temperature spectrum of the SCA powder.²⁶ No indication of conformational changes were observed along all the annealing experiment, which supports the theoretical suggestion (*vide supra*) of the sole presence in the matrix of the most stable *E*-enol conformer I.

Considering the very good agreement between the experimental and theoretically predicted spectra, the assignment of the bands (Table 2) is straightforward. In the high-frequency range (Figure S1), the carboxylic $\nu\text{O}-\text{H}$ stretching band is observed at ca. 3574 cm⁻¹, at a frequency typical of a free OH carboxylic group adopting the *cis* conformation (predicted value for SCA: 3565 cm⁻¹).⁴¹⁻⁴³ The stretching vibration of the hydrogen-bonded phenolic OH group is predicted by the calculations to give rise to a very intense infrared band at 3072 cm⁻¹. Due to the involvement in the hydrogen bond, however, and as found in other similar systems,^{43,44} one can expect the corresponding experimental band to be very broad and spread a wide wavenumber range. Accordingly, a broad feature extended from ca. 3225 to 2625 cm⁻¹ is observed experimentally, which is assigned to this vibration. The band observed at 3430 cm⁻¹ in the high-frequency spectral range is ascribed to the first overtone of the carbonyl stretching vibration, whose fundamental appears at 1751 cm⁻¹.

The fingerprint region (Figure 3) shows an excellent correspondence between the experimental and theoretical spectra. The main deformation vibrations associated with the hydrogen-bonded phenolic OH group are predicted at 1417 cm⁻¹ (δOH) and 820 cm⁻¹ (τOH) and have correspondence with the bands at 1420/1418 and 810-795 cm⁻¹ in the experimental spectrum. The displacement of the $\tau(\text{OH})$ mode of the phenolic OH group toward considerably higher wavenumbers relatively to the analogous vibration of the carboxylic OH group (observed around 571 cm⁻¹, matching the calculated value; Table 2) is related to the involvement of the first in the intramolecular hydrogen bond. The shift of this type of vibration to higher wavenumbers upon hydrogen bond formation is indeed a general rule, which has been comprehensively addressed elsewhere.⁴⁵ The δOH in-plane bending vibration of the carboxylic group contributes to several absorptions in the fingerprint region, mainly to those predicted at 1334, 1185, and 1155/1151 cm⁻¹, which have experimental

counterparts at 1366/1338 cm⁻¹ (Fermi doublet involving participation of the $\delta\text{OCO} + \tau\text{CC}$ combination tone, whose fundamentals are observed at 653 and around 700 cm⁻¹, the last being a torsional mode of the *p*-carboxyphenyl ring), 1187 cm⁻¹, and in the 1165-1151 cm⁻¹ range (complex feature with two different groups of bands also resulting from Fermi interaction with the carboxylic τOH first overtone). The $\nu\text{C}=\text{N}$ stretching mode of the azomethine group is predicted at 1630 cm⁻¹ and observed at ca. 1622 cm⁻¹, whereas the CH bending modes (in-plane, δCH , and out-of-the-plane, γCH) of the same fragment were predicted at 1367 and 984 cm⁻¹ and observed at 1359 and at 985 cm⁻¹. The azomethine $\nu\text{C}-\text{H}$ stretching mode is predicted at 2872 cm⁻¹ and is tentatively assigned to the bands at 2869/2862 cm⁻¹, though the usual low intensity of the bands due to CH stretching modes in the spectra of Ar-matrix isolated molecules prevents a definitive assignment.

One additional note shall be made here, calling attention to the fact that several bands in the SCA Ar-matrix spectrum are observed as multicomponent peaks, as it occurs most of times in the spectra of matrix-isolated molecules due to the existence of multiple matrix trapping sites. This is observed all along the spectrum of the compound, but it is particularly noticeable for the most intense bands, which are in most cases associated with the more polarized groups in the molecule, whose internal vibrational potentials are more sensitive to interactions with the matrix atoms (namely, the bands associated with the phenolic OH group and the carboxylic substituent).

3.3. Unimolecular Photochemistry of SCA in an Argon Matrix. The photochemical reactions experienced by SCA molecules in cryogenic conditions were the subject of two experiments: by using tunable UV light from a laser/MOPO system, or exposing the sample to the broad-band light emitted by a high-pressure Hg(Xe) lamp through the outer KBr window of the cryostat ($\lambda > 235$ nm). The first experimental approach used irradiations at 335 and 345 nm, which lie near the absorption maximum of the UV/visible absorbance spectrum of SCA (*E*-enol form).²⁹

The changes observed in the infrared spectrum of SCA upon the different irradiations ($\lambda > 235$, or $\lambda = 335$; 345 nm) were found to be similar, though a faster consumption of the reactant was observed upon broad-band irradiation. Figures 4-6 show the IR difference spectra (in three different spectral regions) resulting from subtracting the spectrum of the as-deposited matrix, containing exclusively the *E*-enol form, from the spectrum registered after 20 min of irradiation at $\lambda = 335$ nm followed by 30 min of irradiation at 345 nm, and from the spectrum obtained after 1 min of broad-band irradiation ($\lambda > 235$ nm). The results obtained upon laser/MOPO irradiation at 335 and 345 nm were qualitatively identical, with the shorter wavelength being slightly more efficient in promoting the photochemical transformations than the longer one. The broad-band irradiation was very effective, with consumption of practically all reactant in the first minute of irradiation. Prolonged broad-band irradiation led to observation of characteristic bands of CO₂ (ca. 2340 cm⁻¹)⁴⁶ and CO (about 2130 cm⁻¹),⁴⁷ demonstrating occurrence of both photodecarboxylation and photodecarbonylation reactions. These bands were, however, completely absent from the infrared spectrum obtained after 1 min of broad-band

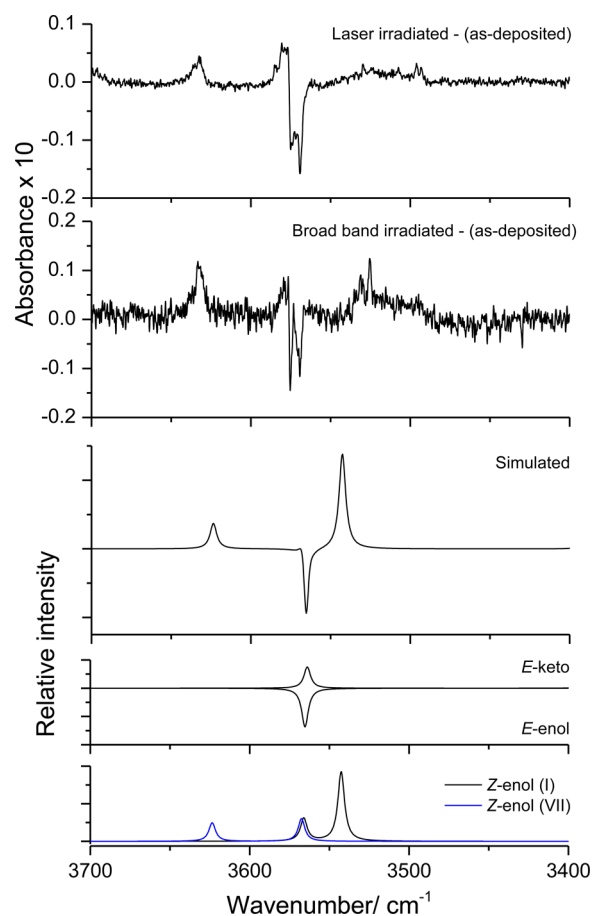


Figure 4. From bottom to top: calculated infrared spectra of conformers I (black) and VII (blue) of the Z-enol; calculated infrared spectra of *E*-keto (bands pointing up) and *E*-enol most stable conformers; simulated difference spectrum built from the calculated infrared spectra: $0.5 \times E\text{-keto} + 0.5 \times (Z\text{-enol I} + Z\text{-enol VII}) - E\text{-enol}$; experimental infrared difference spectrum: matrix irradiated for 1 min with the broad-band light of the Hg(Xe) lamp ($\lambda > 235$ nm) minus as-deposited matrix; experimental infrared difference spectrum: matrix irradiated for 20 min of irradiation at $\lambda = 335$ nm followed by 30 min at $\lambda = 345$ nm with laser light minus as-deposited matrix. All calculated spectra were obtained at the B3LYP/6-311++G(d,p) level of theory and the wavenumbers were scaled by 0.945; the bands were simulated by Lorentzian functions centered at the scaled calculated frequency and with full-width-at-half-band of 5 cm^{-1} .

irradiation, indicating that the photodecomposition reactions occurred from the initially formed photoproducts and not from the *E*-enol reactant (this does not mean that the *E*-enol species cannot also undergo photodecarboxylation or photodecarbonylation, but just that these are much slower processes compared to those occurring extensively during the first minute of irradiation).

Systematic comparison of the bands due to the photo-produced species with the calculated spectra of all SCA isomeric species (all investigated conformers of *E*- and Z-enol and *E*- and Z-keto forms; see Table S3 in the Supporting Information for calculated spectra for all these species) allowed us to identify the products of the photoinduced reactions. This identification was made on the basis of the full spectral range (assignments are given in Table 2). However, the bands observed at 3632 cm^{-1} and in the $3540\text{--}3490\text{ cm}^{-1}$ region (Figure 4), at 1531 , 1516 , and 1258 cm^{-1} (Figure 5), and at 712 cm^{-1} (Figure 6) proved to be instrumental for this task. In

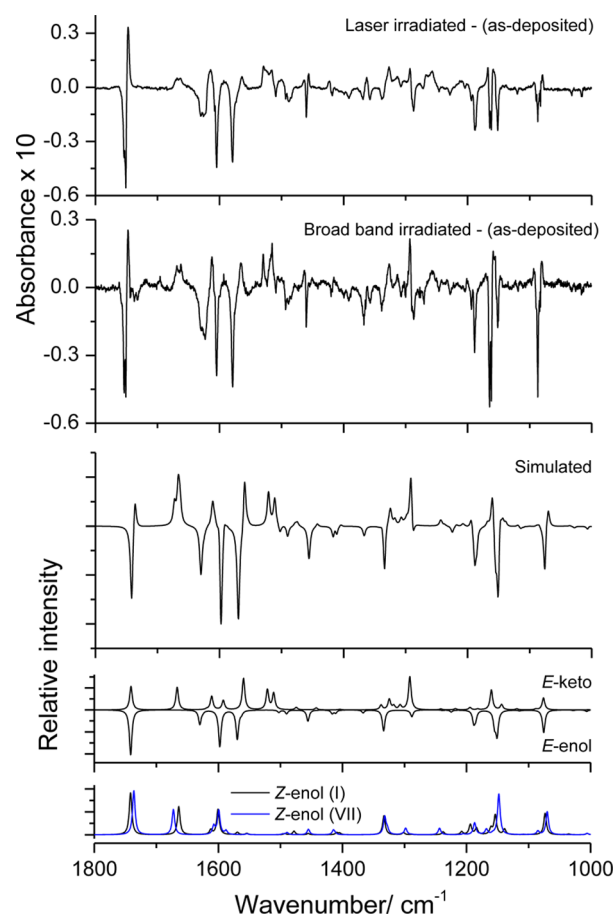


Figure 5. From bottom to top: calculated infrared spectra of conformers I (black) and VII (blue) of the Z-enol; calculated infrared spectra of *E*-keto (bands pointing up) and *E*-enol most stable conformers; simulated difference spectrum built from the calculated infrared spectra: $0.5 \times E\text{-keto} + 0.5 \times (Z\text{-enol I} + Z\text{-enol VII}) - E\text{-enol}$; experimental infrared difference spectrum: matrix irradiated for 1 min with the broad-band light of the Hg(Xe) lamp ($\lambda > 235$ nm) minus as-deposited matrix; experimental infrared difference spectrum: matrix irradiated for 20 min of irradiation at $\lambda = 335$ nm followed by 30 min at $\lambda = 345$ nm with laser light minus as-deposited matrix. All calculated spectra were obtained at the B3LYP/6-311++G(d,p) level of theory and the wavenumbers were scaled by 0.978; the bands were simulated by Lorentzian functions centered at the scaled calculated frequency and with full-width-at-half-band of 5 cm^{-1} .

the following discussion, the above-mentioned fact that all pairs of structures differing only in the orientation of the carboxylic substituent are spectroscopically indiscernible will be taken into account.

The band at 3632 cm^{-1} appears at a characteristic frequency of an OH stretching vibration of a non-hydrogen-bonded phenolic moiety,^{48,49} being indicative of photoproduction of an enol-type species where the OH phenol group is free. Conformers III–VIII of the *E*-enol and III–VIII of the Z-enol obey this condition. However, the *E*-enol forms can be safely discarded, because all of them have characteristic intense bands (according to the theoretical predictions) that are not present in the spectra of the irradiated matrixes: for the *E*-enol conformers III/IV bands at 1580 and 1102 cm^{-1} , for conformers V–VIII bands in the $1595\text{--}1585$ and $1230\text{--}1220\text{ cm}^{-1}$ regions (all these bands corresponding to vibrations with significant contributions from the phenolic δCOH or $\nu\text{C}\text{--O}$ coordinate). The remaining intense bands of these forms are

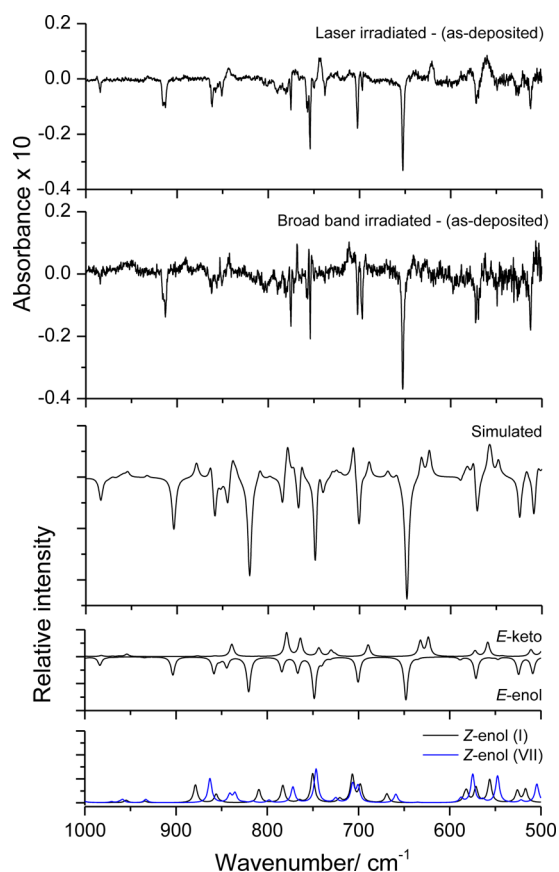


Figure 6. From bottom to top: calculated infrared spectra of conformers I (black) and VII (blue) of the Z-enol; calculated infrared spectra of E-keto (bands pointing up) and E-enol most stable conformers; simulated difference spectrum built from the calculated infrared spectra: $0.5 \times E\text{-keto} + 0.5 \times (Z\text{-enol I} + Z\text{-enol VII}) - E\text{-enol}$; experimental infrared difference spectrum: matrix irradiated for 1 min with the broad-band light of the Hg(Xe) lamp ($\lambda > 235$ nm) minus as-deposited matrix; experimental infrared difference spectrum: matrix irradiated for 20 min of irradiation at $\lambda = 335$ nm followed by 30 min at $\lambda = 345$ nm with laser light minus as-deposited matrix. All calculated spectra were obtained at the B3LYP/6-311++G(d,p) level of theory and the wavenumbers were scaled by 0.978; the bands were simulated by Lorentzian functions centered at the scaled calculated frequency and with full-width-at-half-band of 5 cm^{-1} .

nearly coincident with bands due to other species. On the contrary, all the Z-enol forms III–VIII can *a priori* be present in the irradiated sample, because they do not have any characteristic intense band predicted by the theory at a frequency where no bands are observed in the experimental spectra. One can, however, suppose that, even if all these Z-enol conformers are present (and, as it will be pointed out below, there are reasons to think they are not), the lowest energy conformer VII shall dominate.

The broad feature observed in the $3540\text{--}3490\text{ cm}^{-1}$ region of the spectrum of the irradiated matrixes (Figure 4) can only be originated in the Z-enol pair of conformers I/II, because both its frequency range and the observed broad profile are very characteristic of a stretching mode of a phenolic O–H group involved in a weak hydrogen bond. Preferential formation of Z-enol I from the irradiated E-enol I species seems in fact to be rather plausible, because it requires just the $E \rightarrow Z$ isomerization to take place without any other

(simultaneous or subsequent) conformational rearrangement (Figure 1A,B).

The bands at 1258 cm^{-1} (Figure 5) and 712 cm^{-1} (Figure 6) in the spectra of the irradiated matrixes are also characteristic of Z-enol forms (according to the calculations they cannot be ascribed to E-enol or the keto isomers), being ascribed to the phenolic $\nu\text{C–O}$ stretching and one of the torsional modes of the *p*-carboxyphenyl ring, and are a further experimental evidence of photoproduction of the Z-enol isomer in the described experiments.

In turn, the pair of bands observed in the spectra of the irradiated matrixes at 1531 and 1516 cm^{-1} cannot be explained by any of the enol isomers (Figure 5), being a particularly clear evidence of the occurrence of the $E\text{-enol} \rightarrow E\text{-keto}$ phototautomerization upon irradiation of matrix-isolated SCA. Indeed, besides these two bands (originated in vibrations with significant contributions from the cyclohexadienone ring stretchings), most of the predicted bands for the E-keto most stable pair of conformers (E-keto I/II forms) are experimentally observed, as can be easily noticed in Figures 4–6.

In summary, the analysis of the results of the performed irradiation experiments on matrix-isolated monomeric SCA E-enol clearly demonstrates the competitive occurrence of simple $E\text{-enol} \rightarrow Z\text{-enol}$ isomerization and $E\text{-enol} \rightarrow E\text{-keto}$ tautomerization. Both processes were found to be rather effective, with practically complete consumption of the reactant after broad-band irradiation ($\lambda > 235$ nm) by 1 min only. With all probability, the first process leads to the initial formation of the Z-enol conformer I, which requires just the E-to-Z isomerization to take place without any additional conformational rearrangement; conformational isomerization shall then occur transforming the Z-enol I into the lowest energy Z-enol conformer VII. Note that among the Z-enol conformers, conformer VII (and its spectroscopically indiscernible pair, VIII) is the only conformer with a lower energy than conformer I, so that formation of the remaining Z-enol conformers seems in fact not very probable. The $E\text{-enol} \rightarrow E\text{-keto}$ tautomerization implies excited state intramolecular proton transfer and twisting about the exocyclic CC bond of the molecule, transforming the initial E-enol form into the E-keto form. The two events (proton transfer and CC twisting) most probably take place sequentially, though there is no convincing spectroscopic evidence of the presence in the irradiated matrixes of the Z-keto form, which should act as intermediate in this sequence of processes (Scheme 1). This can be attributed to the efficiency and fast kinetics of the two processes under the irradiation conditions used, and also because the E-keto form was found to be rather photostable under those conditions, so that no photostationary equilibrium could be reached between the two keto isomers (back conversion should require use of considerably longer excitation wavelength, in the visible range).²⁶

In an attempt to roughly estimate the branching ratio between the $E\text{-enol} \rightarrow Z\text{-enol}$ isomerization and $E\text{-enol} \rightarrow E\text{-keto}$ tautomerization photoinduced processes, one tried to reproduce the experimentally observed infrared difference spectra shown in Figures 4–6 using different combinations of the theoretically predicted infrared spectra of the relevant species (i.e., the reactant E-enol conformer I, and the identified photoproducts, Z-enol conformers I and VII and E-keto form I). The resulting simulated spectrum built by assuming the $E\text{-enol} \rightarrow Z\text{-enol} : E\text{-enol} \rightarrow E\text{-keto}$ branching ratio of 1:1 (with the spectra of the two Z-enol conformers contributing equally)

is represented in Figures 4–6 and shows a very good agreement with the experimental data, indicating that, under the used experimental conditions, the *E*-enol → *Z*-enol isomerization and *E*-enol → *E*-keto tautomerization occur with nearly equal probability.

4. CONCLUSION

The molecular structure and photochemistry of *N*-salicylidene-*p*-carboxyaniline isolated in a cryogenic (15 K) solid argon matrix was investigated. The detailed characterization of the conformational space of the enol-imine and keto-amine tautomers of the compound in both their *E* and *Z* isomeric forms was undertaken. These data, together with the theoretically predicted infrared spectra for the various conformers of the enol-imine and keto-amine SCA forms, were used to interpret the infrared spectrum of the matrix-isolated compound. It was demonstrated that the obtained Ar-matrixes (prepared from the vapors resulting from sublimation of crystalline *E*-enol form) contain only the most stable conformer of the *E*-enol isomer of the compound. Irradiation of the matrixes (either with narrow- or broad-band UV light, at $\lambda = 335$; 345 nm, or $\lambda > 235$ nm, respectively) led to observation of two competing photoreaction channels: *E*-enol → *Z*-enol isomerization and *E*-enol → *E*-keto tautomerization (prolonged broad-band irradiation was found to lead to photofragmentation, with production of CO₂ and CO). Both *E*-enol → *Z*-enol isomerization and *E*-enol → *E*-keto tautomerization reactions were found to be rather effective, with practically complete consumption of the reactant in the first minute of broad-band irradiation.

In the case of the *E*-enol → *Z*-enol isomerization, the presence in the irradiated matrixes of the *Z*-enol conformer that differs from the reactant only by *E*-to-*Z* isomerization suggests the initial photoproduction of this conformer, which then decays into the lowest energy *Z*-enol conformer (also identified experimentally).

The *E*-enol → *E*-keto tautomerization requires the excited state intramolecular proton transfer and twisting about the exocyclic CC bond of the molecule, which most probably takes place sequentially. However, in the present study the *Z*-keto isomer, which should act as an intermediate in this sequence of processes, could not be detected, most probably due to its short lifetime under the used experimental conditions. On the contrary, the detailed structural and vibrational characterization of the photoproduced *E*-keto form was successfully achieved.

The branching ratio for the two observed competing photoreaction channels was estimated as ~1:1. Such a branching ratio differs from what was found for the compound in the crystalline state,²⁶ where the *E*-enol → *E*-keto tautomerization dominates. In turn, this supports the idea²⁶ that the characteristic photochromic properties of the compound are substantially affected by the molecular surroundings.

■ ASSOCIATED CONTENT

Supporting Information

The Supporting Information is available free of charge on the ACS Publications website at DOI: 10.1021/acs.jpca.5b06516.

Figures showing the high-frequency range of the infrared spectrum of the as-deposited SCA argon matrix and the B3LYP/6-311++G(d,p) calculated infrared spectrum of the most stable *E*-enol conformer, B3LYP/6-311+

+G(d,p) calculated infrared spectra for the most stable conformer of the four different tautomers of SCA, B3LYP/6-311++G(d,p) calculated infrared spectra of the *E*-enol conformers I and II (full range). Tables of the most characteristic dihedral angles for the various conformers of SCA, B3LYP/6-311++G(d,p) calculated Cartesian coordinates for the optimized structures, and infrared spectra of the various conformers of SCA (PDF)

■ AUTHOR INFORMATION

Corresponding Author

*R. Fausto E-mail: rfausto@ci.uc.pt.

Notes

The authors declare no competing financial interest.

■ ACKNOWLEDGMENTS

The authors gratefully acknowledge Fundação para a Ciência e a Tecnologia (FCT), through the projects PEst-OE/QUI/UI0313/2014 (Coimbra Chemistry Centre), cofunded by QREN-COMPETE-UE. Financial support has been also provided within the framework of the FCT postdoctoral grant SFRH/BPD/88372/2012 (N.K.).

■ REFERENCES

- (1) Irie, M. Photochromism: Memories and Switches – Introduction. *Chem. Rev.* **2000**, *100*, 1683–1684.
- (2) Delaire, J. A.; Nakatani, K. Linear and Nonlinear Optical Properties of Photochromic Molecules and Materials. *Chem. Rev.* **2000**, *100*, 1817–1845.
- (3) Staehle, I. O.; Rodríguez-Molina, B.; Khan, S. I.; Garcia-Garibay, M. A. Engineered Photochromism in Crystalline Salicylidene Anilines by Facilitating Rotation to Reach the Colored *trans*-Keto Form – I. *Cryst. Growth Des.* **2014**, *14*, 3667–3673.
- (4) Kownacki, K.; Mordzinski, A.; Wilbrandt, R.; Grabowska, A. Laser-Induced Absorption and Fluorescence Studies of Photochromic Schiff Bases. *Chem. Phys. Lett.* **1994**, *227*, 270–276.
- (5) Ziółek, M.; Kubicki, J.; Maciejewski, A.; Naskręcki, R.; Grabowska, A. An Ultrafast Excited State Intramolecular Proton Transfer (ESIPT) and Photochromism of Salicylideneaniline (SA) and Its “Double” Analogue Salicylaldehyde Azine (SAA). A Controversial Case. *Phys. Chem. Chem. Phys.* **2004**, *6*, 4682–4689.
- (6) Sliwa, M.; Mouton, N.; Ruckebusch, C.; Poisson, L.; Idrissi, A.; Aloïse, S.; Potier, L.; Dubois, J.; Poizat, O.; Buntinx, G. Investigation of Ultrafast Photoinduced Processes for Salicylidene Aniline in Solution and Gas Phase: Toward a General Photo-Dynamical Scheme. *Photochem. Photobiol. Sci.* **2010**, *9*, 661–669.
- (7) Asahi, T.; Masuhara, H.; Nakatani, K.; Sliwa, M. Photochromic Dynamics of Salicylidene Aniline in Solid State by Using Femtosecond Transient Absorption Spectroscopy. *Mol. Cryst. Liq. Cryst.* **2005**, *431*, 541–548.
- (8) Harada, J.; Ogawa, K. Pedal Motion in Crystals. *Chem. Soc. Rev.* **2009**, *38*, 2244–2252.
- (9) Mitra, S.; Tamai, N. Femtosecond Spectroscopic Study on Photochromic Salicylideneaniline. *Chem. Phys. Lett.* **1998**, *282*, 391–397.
- (10) Mitra, S.; Tamai, N. Dynamics of Photochromism in Salicylideneaniline: A Femtosecond Spectroscopic Study. *Phys. Chem. Chem. Phys.* **2003**, *5*, 4647–4652.
- (11) Zgierski, M. Z.; Grabowska, A. Photochromism of Salicylideneaniline SA. How the photochromic Transient is Created: A Theoretical Approach. *J. Chem. Phys.* **2000**, *112*, 6329–6337.
- (12) Rodríguez-Córdoba, W.; Zugazagoitia, J. S.; Collado-Fregoso, E.; Peon, J. Excited State Intramolecular Proton Transfer in Schiff Bases. Decay of the Locally Excited Enol State Observed by Femtosecond Resolved Fluorescence. *J. Phys. Chem. A* **2007**, *111*, 6241–6247.

- (13) Ortiz-Sánchez, J. M.; Gelabert, R.; Moreno, M.; Lluch, J. M. Electronic-Structure and Quantum Dynamical Study of the Photochromism of the Aromatic Schiff Base Salicylideneaniline. *J. Chem. Phys.* **2008**, *129* (214308), 1–11.
- (14) Ziółek, M.; Kubicki, J.; Maciejewski, A.; Naskrecki, R.; Grabowska, A. Enol-Keto Tautomerism of Aromatic Photochromic Schiff Base N,N'-bis-salicylidene-*p*-Phenylenediamine: Ground State Equilibrium and Excited State Deactivation Studied by Solvatochromic Measurements on Ultrafast Time Scale. *J. Chem. Phys.* **2006**, *124* (124518), 1–10.
- (15) Ziółek, M.; Burdzinski, G.; Filipczak, K.; Karolczak, J.; Maciejewski, A. Spectroscopic and Photophysical Studies of the Hydroquinone Family of Photochromic Schiff Bases Analyzed Over a 17-Orders-of-Magnitude Time Scale. *Phys. Chem. Chem. Phys.* **2008**, *10*, 1304–1318.
- (16) Grzegorzec, J.; Filarowski, A.; Mielke, Z. The Photoinduced Isomerization and Its Implication in the Photo-Dynamical Processes in Two Simple Schiff Bases Isolated in Solid Argon. *Phys. Chem. Chem. Phys.* **2011**, *13*, 16596–16605.
- (17) Ogawa, K.; Harada, J. Aggregation Controlled Proton Tautomerization in Salicylideneanilines. *J. Mol. Struct.* **2003**, *647*, 211–216.
- (18) Turbeville, W.; Dutta, P. K. Spectroscopic Studies of the Photochromic Molecule N-(2-Hydroxybenzylidene)aniline and Its Photoproduct. *J. Phys. Chem.* **1990**, *94*, 4060–4066.
- (19) Lewis, J. W.; Sandorfy, C. A Spectroscopic Study of Proton Transfer and Photochromism in N-(2-Hydroxybenzylidene)aniline. *Can. J. Chem.* **1982**, *60*, 1738–1746.
- (20) Yuzawa, T.; Takahashi, H.; Hamaguchi, H. Submicrosecond Time-Resolved Infrared Study on the Structure of the Photoinduced Transient Species of Salicylideneaniline in Acetonitrile. *Chem. Phys. Lett.* **1993**, *202*, 221–226.
- (21) Ruckebusch, C.; Sliwa, M.; Réhault, J.; Naumov, P.; Huvenne, J. P.; Buntinx, G. Hybrid Hard- and Soft-Modelling Applied to Analyze Ultrafast Processes by Femtosecond Transient Absorption Spectroscopy: Study of the Photochromism of Salicylidene Anilines. *Anal. Chim. Acta* **2009**, *642*, 228–34.
- (22) Pajak, J.; Maes, G.; De Borggraeve, W. M.; Boens, N.; Filarowski, A. Matrix-Isolation FT-IR and Theoretical Investigation of the Competitive Intramolecular Hydrogen Bonding in 5-Methyl-3-nitro-2-hydroxyacetophenone. *J. Mol. Struct.* **2008**, *880*, 86–96.
- (23) Pajak, J.; Maes, G.; De Borggraeve, W. M.; Boens, N.; Filarowski, A. Matrix-Isolation FT-IR and Theoretical Investigation of the Vibrational Properties of the Sterically Hindered *Ortho*-Hydroxy Acylaromatic Schiff Bases. *J. Mol. Struct.* **2007**, *844/845*, 83–93.
- (24) Grzegorzec, J.; Mielke, Z.; Filarowski, A. C=N-N=C Conformational Isomers of 20-Hydroxyacetophenone Azine: FTIR Matrix Isolation and DFT Study. *J. Mol. Struct.* **2010**, *976*, 371–376.
- (25) Grzegorzec, J.; Mielke, Z. Photochemistry of Salicylaldehyde in Solid Argon: An Experimental and Theoretical Study. *Eur. J. Org. Chem.* **2010**, *27*, 5301–5309.
- (26) Avadanei, M.; Cozan, V.; Shova, S.; Paixão, J. A. Solid State Photochromism and Thermochromism of Two Related N-Salicylidene Anilines. *Chem. Phys.* **2014**, *444*, 43–51.
- (27) Hadjoudis, E.; Mavridis, I. M. Photochromism and Thermochromism of Schiff Bases in the Solid State: Structural Aspects. *Chem. Soc. Rev.* **2004**, *33*, 579–588.
- (28) Chen, X.-T.; Xiang, Y.; Song, P.-S.; Wei, R.-R.; Zhou, Z.-J.; Li, K.; Tong, A.-J. *p*-Carboxyl-N-salicylideneanilines: Simple But Efficient Chromophores for One-Dimensional Microrods With Aggregation-Induced Emission Enhancement (AIEE) Characteristics. *J. Lumin.* **2011**, *131*, 1453–1459.
- (29) Johmoto, K.; Sekine, A.; Uekusa, H. Photochromism Control of Salicylideneaniline Derivatives by Acid-Base Co-Crystallization. *Cryst. Growth Des.* **2012**, *12*, 4779–4786.
- (30) Becke, A. D. Density-Functional Exchange-Energy Approximation with Correct Asymptotic Behavior. *Phys. Rev. A: At, Mol, Opt. Phys.* **1988**, *38*, 3098–3100.
- (31) Lee, C.; Yang, W.; Parr, R. G. Development of the Colle-Salvetti Correlation-Energy Formula into a Functional of the Electron Density. *Phys. Rev. B: Condens. Matter Mater. Phys.* **1988**, *37*, 785–789.
- (32) McLean, A. D.; Chandler, G. S. Contracted Gaussian-basis Sets for Molecular Calculations. I. 2nd row atoms, Z=11–18. *J. Chem. Phys.* **1980**, *72*, 5639–5648.
- (33) Frisch, M. J.; Trucks, G. W.; Schlegel, H. B.; Scuseria, G. E.; Robb, M. A.; Cheeseman, J. R.; Scalmani, G.; Barone, V.; Mennucci, B.; Petersson, G. A.; et al. *Gaussian 09*, Revision A.02; Gaussian, Inc.: Wallingford, CT, 2009.
- (34) Teixeira-Dias, J. J. C.; Fausto, R. A Molecular Mechanics Force Field for Conformational Analysis of Simple Acyl Chlorides, Carboxylic Acids and Esters. *J. Mol. Struct.* **1986**, *144*, 199–213.
- (35) Fausto, R.; Teixeira-Dias, J. J. C. The High Energy *s-trans* Conformers of CH₃COOH and CH₃COOCH₃: A Molecular Mechanics and Vibrational Study of CH₃COCl, CH₃COOH and CH₃COOCH₃. *J. Mol. Struct.* **1986**, *144*, 215–223.
- (36) Teixeira-Dias, J. J. C.; Batista de Carvalho, L. A. E.; Fausto, R. The C_α-C Internal Rotation in α -Alkyl Substituted Carbonyls and Thiocarbonyls: CH(CH₃)₂C(=X)YH (X,Y= O or S). *J. Comput. Chem.* **1991**, *12*, 1047–1057.
- (37) Fausto, R.; Matos Beja, A. M.; Paixão, J. A. Molecular Structure and Charge Density Analysis of *p*-Methoxybenzoic Acid (Anisic Acid). *J. Mol. Struct.* **1997**, *435*, 207–218.
- (38) Rosado, M. T. S.; Lopes Jesus, A. J.; Reva, I. D.; Fausto, R.; Redinha, J. S. Conformational Cooling Dynamics in Matrix-Isolated 1,3-Butanediol. *J. Phys. Chem. A* **2009**, *113*, 7499–7507.
- (39) Reva, I. D.; Stepanian, S. G.; Adamowicz, L.; Fausto, R. Missing Conformers: Comparative Study of Conformational Cooling in Cyanoacetic Acid and Methyl Cyanoacetate Isolated in Low Temperature Inert Gas Matrixes. *Chem. Phys. Lett.* **2003**, *374*, 631–638.
- (40) Barnes, A. J. Matrix Isolation Vibrational Spectroscopy as a Tool for Studying Conformational Isomerism. *J. Mol. Struct.* **1984**, *113*, 161–174.
- (41) Maçôas, E. M. S.; Kriachtchev, L.; Pettersson, M.; Fausto, R.; Räsänen, M. Rotational Isomerism in Acetic Acid: The First Experimental Observation of the High-Energy Conformer. *J. Am. Chem. Soc.* **2003**, *125*, 16188.
- (42) Maçôas, E. M. S.; Kriachtchev, L.; Pettersson, M.; Fausto, R.; Räsänen, M. Internal Rotation in Propionic Acid: Infrared Induced Isomerization in Solid Argon. *J. Phys. Chem. A* **2005**, *109*, 3617–3625.
- (43) Kuş, N.; Sharma, A.; Pena, I.; Bermúdez, M.; Cabezas, C.; Alonso, J.; Fausto, R. Conformers of β -Aminoisobutyric Acid Probed by Jet-Cooled Microwave and Matrix Isolation Infrared Spectroscopic Techniques. *J. Chem. Phys.* **2013**, *138* (144305), 1–10.
- (44) Duarte, L.; Giuliano, B. M.; Reva, I.; Fausto, R.; Tautomers. and UV-Induced Photoisomerization of a Strongly Intramolecularly H-Bonded Aromatic Azo-Dye: 1-(Cyclopropyl)diazo-2-Naphthol. *J. Phys. Chem. A* **2013**, *117*, 10671–10680.
- (45) Rozenberg, M.; Shoham, G.; Reva, I.; Fausto, R. A Correlation Between the Proton Stretching Vibration Red Shift and the Hydrogen Bond Length in Polycrystalline Amino Acids and Peptides. *Phys. Chem. Chem. Phys.* **2005**, *7*, 2376–2383.
- (46) Svensson, T.; Nelander, B.; Karlström, G. The CO₂ Complexes with HOO and HO in Argon Matrices. *Chem. Phys.* **2001**, *265*, 323–333.
- (47) Abe, H.; Takeo, H.; Yamada, K. M. T. Infrared Spectroscopy of CO Trapped in an Argon Matrix Revisited. *Chem. Phys. Lett.* **1999**, *311*, 153–158.
- (48) Giuliano, B. M.; Reva, I.; Lapinski, L.; Fausto, R. Infrared Spectra and Ultraviolet-Tunable Laser Induced Photochemistry of Matrix-Isolated Phenol and Phenol-d₅. *J. Chem. Phys.* **2012**, *136* (024505), 1–11.
- (49) Lapinski, L.; Rostkowska, H.; Reva, I.; Fausto, R.; Nowak, M. J. Positive Identification of UV-Generated, Non-Hydrogen-Bonded Isomers of *o*-Hydroxybenzaldehyde and *o*-Hydroxyacetophenone. *J. Phys. Chem. A* **2010**, *114*, 5588–5595.